Appl. Phys. B 85, 235–241 (2006)
DOI: 10.1007/s00340-006-2407-7

Applied Physics B
Lasers and Optics

J.B. MCMANUS[1,✉]
D.D. NELSON[1]
S.C. HERNDON[1]
J.H. SHORTER[1]
M.S. ZAHNISER[1]
S. BLASER[2]
L. HVOZDARA[2]
A. MULLER[2]
M. GIOVANNINI[3]
J. FAIST[3]

Comparison of cw and pulsed operation with a TE-cooled quantum cascade infrared laser for detection of nitric oxide at 1900 cm^{-1}

[1] Aerodyne Research, Inc., 45 Manning Road, Billerica, MA 01821-3976, USA
[2] Alpes Lasers SA, 1–3 Passage Maximilien-de-Meuron, 2000 Neuchâtel, Switzerland
[3] Physics Institute, University of Neuchâtel, 1 A.-L. Breguet, 2000 Neuchâtel, Switzerland

Received: 2 June 2006/Revised version: 29 June 2006
Published online: 16 August 2006 • © Springer-Verlag 2006

ABSTRACT A quantum cascade laser operating near room temperature with thermoelectric (TE) cooling has been used in both continuous-wave (cw) mode (−9 °C) and pulsed mode (+45 °C) to detect atmospheric nitric oxide using spectral lines at 1900.07 cm^{-1} (5.3 μm). The totally non-cryogenic spectrometer integrates the laser with a 69-m astigmatic multi-pass cell and a TE-cooled infrared detector to enable operation for extended time periods without operator attention. The pattern of reflections on the astigmatic cell mirrors has been designed to minimize optical interference fringes, which are substantially greater with cw mode than with pulsed operation. The detection method uses direct absorption with rapid- scan sweep integration to achieve sub-second time response. Detection precision for NO in air of 0.5 parts in 10^9 $\mathrm{Hz}^{-1/2}$ (1σ) is obtained in pulsed mode with an Allan variance minimum corresponding to 0.1 parts in 10^9 after 30-s averaging time. The precision in cw mode improves to 0.1 parts in 10^9 $\mathrm{Hz}^{-1/2}$ and 0.03 parts in 10^9 after 30-s averaging, corresponding to an absorbance per unit path length of 2×10^{-10} cm^{-1}. The advantages and disadvantages of cw compared to pulsed operation are discussed.

PACS 07.88.+y; 42.62.Fi; 82.80.Gk; 92.60.Sz

1 Introduction

Recent advances in quantum cascade (QC) laser technology have extended the temperature range of these devices to permit continuous-wave (cw) operation near room temperature (RT) [1–4]. Measurements of atmospheric nitric oxide using these devices have recently been reported [5–7]. The advent of cw RT QC laser operation offers higher power and narrower laser line widths in the spectral region where molecular absorptions are strongest. Higher power permits sensitive detection of gaseous species using thermoelectrically (TE)-cooled infrared detectors. Narrow line width (compared to pulsed operation) enhances absorption depth for a given trace-gas concentration and improves discrimination of the targeted species from nearby interfering absorption features.

Pulsed operation retains some advantages. Pulsed lasers are presently less expensive to fabricate and can be used with less expensive electronic driver and protection circuits, which can reduce the overall cost of the spectrometer. Pulsed mode can also result in a reduction in the optical interference fringes which often limit overall performance in practical applications of baseline-limited absorbance spectroscopy. High-precision detection of atmospheric trace gases with pulsed-QC lasers at room temperature has been demonstrated and utilized in field experiments [8–11].

We previously reported initial results using a cw RT QCL with nitric oxide absorption at 5.3 μm, and here expand on those findings. In that earlier paper [7], we described cw operation of the same TE-cooled laser in a spectrometer instrument with a TE-cooled detector. The laser showed narrow line width ($\leq 0.0004\,\mathrm{cm}^{-1}$ HWHM) and high single-mode purity $\geq 99.99\%$. The detection sensitivity for NO in a 210-m cell was 0.03 parts in 10^9 (1σ) with a 30-s integration time. In this paper we compare cw and pulsed modes of operation using the same laser as our earlier report but with a different optical system with a shorter path length absorption cell. Particular emphasis is placed on the design of the multiple-pass absorption cell to minimize the effects of optical fringes encountered with cw operation. We achieve a reduction in noise using cw mode to obtain a similar detection sensitivity with a 70-m path length in 0.5 l as was earlier achieved with a 210-m 5.0 l cell. The identical system is used to compare the advantages and disadvantages of cw vs. pulsed operation.

2 Experimental design

The basic experimental design is to measure nitric oxide in ambient air using both pulsed and cw operation with the same optical system and substantially similar electronic control and signal processing systems. While the laser drive circuit differs between the cw and pulsed cases, the measurements are conducted in the same manner, by direct absorption. We rapidly sweep the laser across an absorption feature and perform spectral fits based on calculated absorption profiles [12] to derive mixing ratios. The best state of the laser for measurement involves balancing several parameters, which differ for cw and pulsed operation. Balancing parameters in pulsed operation involves primarily maximizing the power and minimizing the laser line width. As the laser is driven higher above threshold the power increases, but the line width also eventually increases, reducing spectral con-

---

✉ Fax: +1-978-663-4918, E-mail: mcmanus@aerodyne.com

trast. With cw operation, line width limiting mechanisms are current and temperature fluctuations, so the laser line width is much narrower and is not a strong function of laser power.

2.1 *Laser design*

The laser, grown by molecular beam epitaxy (MBE), is designed with an active region based on a bound-to-continuum structure [13] giving emission around 5.3 μm. The heterostructure consists of strain-compensated $In_{0.6}Ga_{0.4}As$/ $In_{0.44}Al_{0.56}As$ layers on an n-doped InP substrate. The strain is continuously varied in each period by a digital alloy technique to increase the upper-state confinement and therefore decrease the leakage current. The laser gain medium consists of 22 periods, containing a partially n-doped injector (Si, $n = 2.0 \times 10^{17}\,\mathrm{cm}^{-3}$) and an undoped four- quantum-well region, similar to the structure published previously [2]. The lower and upper InGaAs claddings (grown by MBE) as well as the InP top cladding (grown by metalorganic vapor phase epitaxy) are the same as in Blaser et al. [2]. The single-mode operation of the laser is created by a distributed feedback (DFB) grating with a period of 830.3 nm etched in the upper InGaAs cladding.

The laser used in these spectroscopic measurements has a DFB grating, mounted junction up, with a waveguide 1.5-mm long and 12-μm wide. Initial characterization was performed with the laser mounted on a TE-cooled holder, allowing measurement of output power as a function of base temperature and current. The output optical power was measured by a calibrated thermopile power meter and spectra were recorded using a Fourier transform infrared spectrometer (FTIR) (Brucker Vertex 70) equipped with a pyroelectric detector. As shown in Fig. 1, this particular laser exhibits a maximum output power of 15.5 mW at −30 °C and 0.4 mW at +20 °C. The threshold current densities at these temperature extremes are 2.2 and 3.3 kA/cm^2, respectively. The temperature dependence of the cw threshold current density leads to a characteristic temperature of $T_0 = 129$ K. The best lasers of the same process exhibit output power as high as 60 mW and can operate up to 30 °C [14].

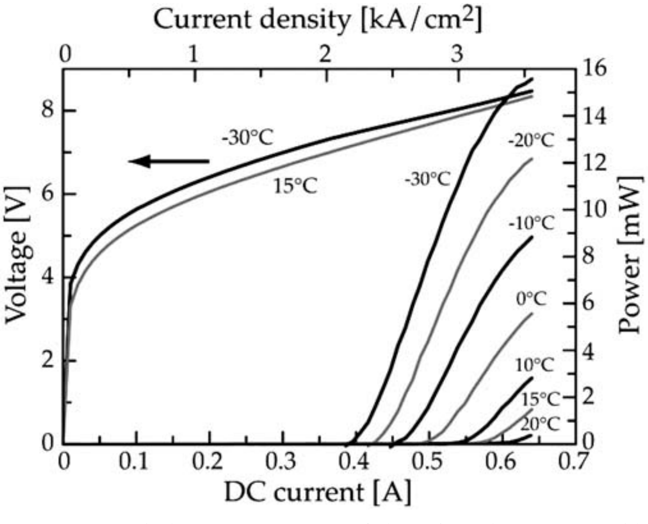

FIGURE 1 Optical power vs. current of the 1.5-mm-long, 12-μm-wide DFB laser in cw mode for various heat-sink temperatures ranging from −30 °C to 20 °C and its voltage vs. current curves at −30 °C and 15 °C

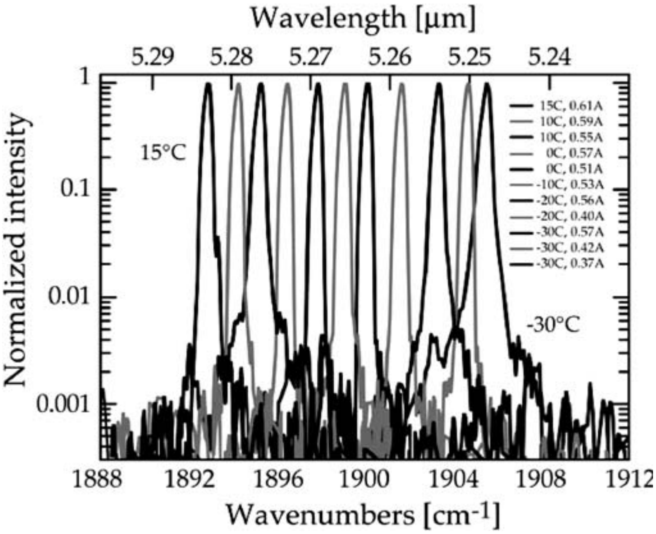

FIGURE 2 High-resolution single-mode cw spectra as a function of temperature and injection current between −30 °C and 15 °C (from the *right* to the *left*)

Continuous-wave laser spectra collected using the FTIR are shown in Fig. 2. Single-mode emission is observed over the entire investigated temperature and current ranges, with a side-mode suppression ratio (SMSR) > 25 dB and a line width narrower than 0.2 cm^{-1} (FWHM), limited by the spectrometer resolution. The monomode emission spectra between −30 °C and 15 °C reveal a tuning range between 1892.9 cm^{-1} and 1905.5 cm^{-1} (over 12.6 cm^{-1} or 0.66%), well covering the set of NO absorption lines near 1900 cm^{-1}. These spectral measurements allow us to deduce a specific thermal conductance of the device $G_{\mathrm{th}} = 457\,\mathrm{W/K\,cm^2}$ and a dimensionless tuning coefficient $[1/\nu]\mathrm{d}\nu/\mathrm{d}T = \beta = -8.96 \times 10^{-5}\,\mathrm{K}^{-1}$ [2, 14]. The temperature difference between the active region and the heat sink can then be calculated as varying from 33 to 59 K for heat-sink temperatures from −30 °C to 15 °C and input electrical power ranging from 2.7 to 4.9 W. The efficiency of conversion from electrical to optical power is quite low, on the order of 0.1%.

2.2 *Measurement system*

The primary elements of the comparison measurement system are shown schematically in Fig. 3. The laser is mounted on a TE cooler in a sealed enclosure. The laser drive signals are controlled by a computer running TDL Wintel software. The same computer program analyzes the detected signals in real time. Most of the light from the laser is directed through a multi-pass cell, which provides ∼ 70 m of absorption path length. Some of the light is directed through a short reference gas cell to derive signals used for laser frequency locking. Light is detected by two TE-cooled HgCdZnTe detectors.

The optical system is simple and compact, with baseplate dimensions of $33 \times 63\,\mathrm{cm}^2$. The optical system is similar to that described in an earlier publication [15]. The main difference is that here the wide cone emission from the laser is col-

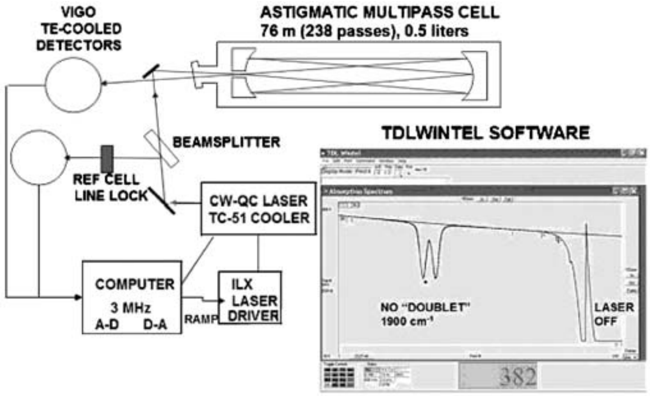

FIGURE 3 QCL spectrometer schematic for cw operation

lected by an off-axis ellipsoid (OAE) [16], which has approximately twice the collection efficiency of the Schwarzchild reflecting objectives that we typically use. Past the OAE there is another stage of magnification to match into the multiple-pass cell [17]. The multiple-pass cell is nominally our standard 76-m 31.5 cm base length cell, but with modifications discussed below. A BaF_2 beam splitter directs $\sim 8\%$ of the light through a short reference gas cell. Simple reflective optics focus light onto the two TE-cooled detectors.

The system for driving the laser and processing the data is similar in both the cw and pulsed cases, with the exception of supplying pulsed current. The pulsed-mode laser drive and signal processing system is similar to that described in detail in an earlier publication [15]. In both cases there is a tuning current ramp that sweeps the laser across the absorption line (tuning range $\sim 0.2\,\mathrm{cm}^{-1}$) at a sweep rate of 2.6 kHz. In the cw case the ramp current (~ 0.5 A) is above threshold, while in the pulsed case the ramp current (~ 0.1 A) is below threshold. The pulsed case has short (~ 10 ns) above-threshold pulses added to the ramp at a rate of ~ 1 MHz. The pulse supplied to the laser is produced by a circuit made by Directed Energy, Inc. (model no. PCO-7120). For cw operation we drive the laser with current from a high-compliance source (ILX LDX-3232) which follows the computer-generated ramp waveform. The ramp and pulse triggers are created by the computer running TDL Wintel. The same program manages synchronous detection of signals and processing of data to report concentrations. The detection bandwidth in the pulsed case is 10 MHz, while in the cw case the bandwidth is 100 kHz. In the pulsed case, we record the integrated transmitted energy for each point in the scan, with the separate pulses well separated. The digitized spectra are averaged and fitted using absorption profiles derived from the HITRAN database [12], at the pressure and temperature of the multiple- pass cell, and accounting for effective laser line width. Absolute concentrations are reported at 1 Hz in these experiments.

3 Multiple pass cell patterns

Interference fringes often limit the useful averaging time and hence the ultimate sensitivity of high-resolution spectroscopic measurements. With the longer coherence length of cw lasers (compared to pulsed), the effect of interferences on the measurement is of increased concern. In these comparison experiments, we have begun to explore a new concept in the application of astigmatic Herriott cells to long path length absorption spectroscopy. We have tested circulation patterns in the cell that are intended to exhibit interference fringes (from mirror scatter) with greater path length differences. Longer length differences produce fringes that are more closely spaced in frequency, which should reduce their deleterious effects.

In infrared absorption measurements, interference fringes with a free spectral range ($\mathrm{FSR} = c/L_f$) close to the absorption line width can be an important source of drift and instability in the derived concentrations. Direct-absorption measurements are based on fitting a line-shape function to the observed optical transmission as the laser frequency (ν_L) is swept across the absorption line. Suppose that the base transmission has an oscillatory structure,

$$T = T_0(1 + A\cos(k\nu_\mathrm{L}))\,, \tag{1}$$

with $k = 2\pi L_\mathrm{f}$ and L_f being the path-length difference producing the interference fringe. The integrated overlap of the line-shape function and the oscillatory baseline indicates the magnitude of the potential error. For the case of a Doppler-broadened line, with absorbance α and width Δ

$$\alpha(\nu_\mathrm{L}) = \alpha_0 \exp\left[-(\nu_L - \nu_0)^2/\Delta^2\right]\,, \tag{2}$$

the overlap has a simple form,

$$\int\limits_{\pm\infty} \exp\left[-(\nu_\mathrm{L} - \nu_0)^2/\Delta^2\right]\cos(k\nu_\mathrm{L})\,\mathrm{d}\nu_\mathrm{L}$$
$$= (\Delta\sqrt{\pi})\exp[-(k\Delta/2)^2]\cos(\varphi)\,, \tag{3}$$

where $\cos(\varphi)$ accounts for the relative phase of absorption line and interference fringe.

The potential error overlap falls by e^{-1} at $k = 2/\Delta$, or $L_\mathrm{f} = 1/(\pi\Delta)$. If the phase of the fringe shifts by one-half period due to thermal drift, then the overlap changes sign and the effect on the retrieved concentration is maximal. Absorption lines of NO near $1900\,\mathrm{cm}^{-1}$ at a pressure of 40 Torr have nearly equal Doppler and collisional broadening, with net broadening of $\sim 0.004\,\mathrm{cm}^{-1}$ (HWHM). With such a line width, the fringe-generating length (at e^{-1} falloff) is ~ 80 cm, or approximately three passes of a cell with a base length of 30 cm. Thus, the most troublesome interference fringes are produced by small pass number differences in the cell.

Alternate pattern selection is based on a model of interference fringes that is under development and which we expect to present in more detail in a forthcoming publication. The fringe model is based on following the propagation of light singly scattered at the mirrors through the cell and to the detector. The strength of the interference fringes is proportional to the square root of the scattered intensity at the detector, and that strength can be evaluated as a function of the path-length difference between the main path and scattered light. The scattered intensity for a given length difference is proportional to the integrated overlap of beam spots on the mirrors, at that length difference. We evaluated numerous patterns that would be available with our existing mirrors and cell body for low overlap of beam spots at low-pass-number differences. Only even pass number differences appear in the detected scattered light, and the lowest significant pass difference is typically four.

The starting configuration for these trials is our standard ARI AMAC-76, with a path length of 76 m, produced by a circulation pattern of 238 passes [17], identified by the parameters $[N, M_x, M_y] = [238, 134, 142]$. With mirror radii of 246 and 269.4 mm, this pattern is available with mirror spacing 321.2 mm and twist ±12.9°. We also compare pulsed and cw laser operation with the cell set up in an alternate pattern, with $[N, M_x, M_y] = [206, 120, 128]$. This pattern is available with mirror spacing of 338.1 mm and twist ±7.1°, for a total path length of 69.65 m. The alternate pattern is selected based on the expectation that it would have reduced low-frequency interference fringes corresponding to four, six, and eight pass differences. The 238-pass pattern is expected to have relatively high fringe levels at four- and 10-pass differences.

We observe clear interference fringe patterns with cw QCL operation, which we do not observe with pulsed operation. Spectral transforms show mixes of generating lengths for the fringe patterns, with some of the lengths associated with the multi-pass cell and some not. An example of an interference pattern produced by a cell is shown in Fig. 4, for the 238-pass pattern. The graph in Fig. 4 is the normalized residual obtained by subtracting the spectrum from a polynomial fit. The Fourier transform of the interference pattern shown in Fig. 4 yields a spectrum of generating lengths, shown in Fig. 5, with the scale on the length spectrum normalized to the cell base length. There are clear peaks in the spectrum of four, 10, and 14 passes, which well match a computation of the dominant length differences produced by mirror scatter, for this circulation pattern. The next example of cell interference is for a cell set to pattern [206, 120, 128]. In this instance a piezoelectric vibrator is mounted behind the rear mirror, which is useful for determining which interferences originate within the cell. Interference patterns obtained with the mirror piezo turned off and on are shown in Fig. 6. With the piezo turned off, the standard deviation of the normalized residual is 1.7×10^{-4}. The lower fringe level in this instance (compared to the 238-pass case) was partially due to an electronic filter (cutoff frequency 100 kHz), and partially due to the pattern. With the cell piezo on, the standard deviation is 2.1×10^{-5}. Fourier transforms of these residuals are shown in Fig. 7. The piezo-off spectrum has clear peaks at four, six, and 10 cell passes, which again are in reasonable agreement with expectations from model calculations, although the six-pass amplitude is higher than expected. The piezo-on spectrum has lower overall power, and the dominant peak corresponds to three passes of the cell. Since odd number pass differences are not allowed, this residual interference originates from outside the cell.

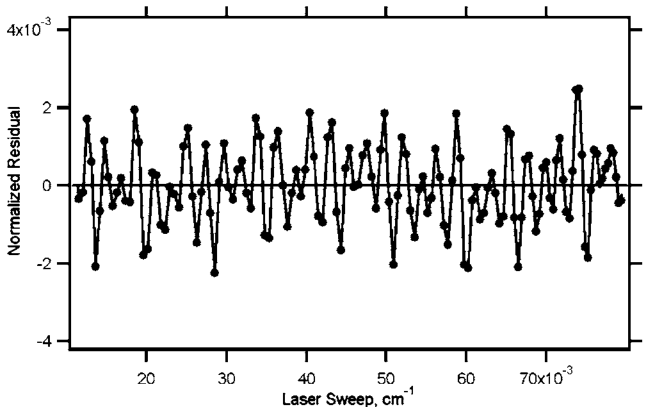

FIGURE 4 Interference pattern observed with the 1900-cm^{-1} cw QC laser in an instrument with a 76-m cell, 238 passes, and base length 32.12 cm. The fluctuations shown are the normalized residual from a polynomial fit to the spectrum, with a standard deviation of 1.1×10^{-3}

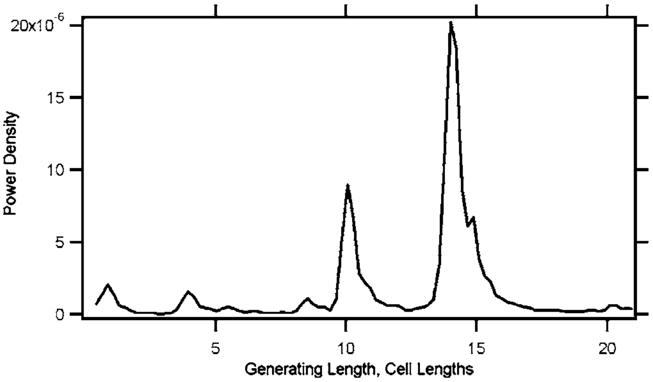

FIGURE 5 Power spectrum of the interference fringes shown in Fig. 4 for a cell set to 238 passes. The length spectrum has been converted to cell lengths by dividing by the base length of 32.12 cm

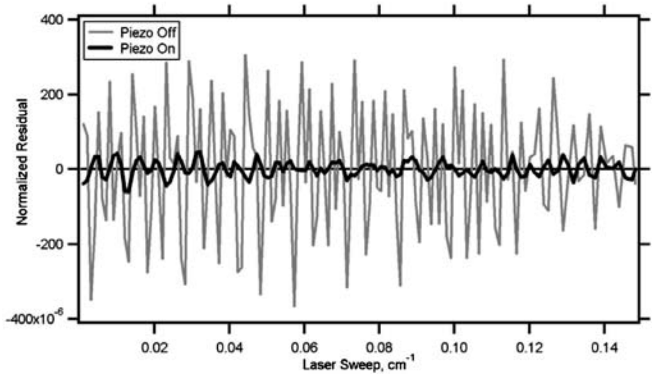

FIGURE 6 Spectral residuals for the 206-pass pattern without and with cell piezo turned on. With the cell piezo off, the standard deviation is 1.7×10^{-4}. With the cell piezo on, the standard deviation is 2.1×10^{-5}

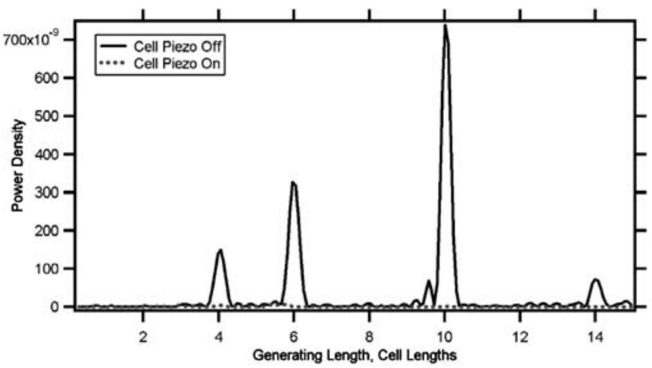

FIGURE 7 Power spectrum of the interference spectrum with the cell set to 206 passes. The *dark solid curve* is with the cell piezo turned off and the *lighter dotted curve* is with the cell piezo turned on

In these experiments we have seen some support for a cell fringe model that allows selection of patterns to preferentially generate higher- frequency fringes. In the 206-pass pattern, the fringe levels were lower, by $\sim 1/2$, compared to the 238-pass pattern under similar conditions. The cw mode detection limits described above were with the 206-pass pattern. Length-component spectra were in fair agreement with model expectations, although the 206-pass pattern had a higher than expected six-pass fringe. The model assumes uniform mirror scatter, but the observed balance of length components could be strongly influenced by a few discrete scattering points. When we applied piezoelectric dither to the back cell mirror the high-frequency structure was suppressed by a factor of ~ 10, but it did not make a discernible difference in the short-term noise or the long-term noise limit. In this case, we conclude that the limiting optical interference originated outside the cell, and that the control of fringes in the cell was good enough that the cell itself was not the stability- limiting element.

4 Results and discussion

The detection sensitivity for nitric oxide has been evaluated using both cw and pulsed operation using the same laser, optical system, TE-cooled detectors, and signal-processing method of direct absorption with sweep integration. Both modes of operation use the same absorption transitions at 1900.07 cm^{-1}. In cw mode, this frequency is obtained at a laser base temperature of −9 °C, while in the pulsed mode the temperature is +45 °C. Under the best available setup conditions, detection precision (1σ) of 0.5 parts in $10^9\,\text{Hz}^{-1/2}$ is obtained in pulsed mode. The precision in cw mode improves to 0.1 parts in $10^9\,\text{Hz}^{-1/2}$ and to 0.03 parts in 10^9 after 30-s averaging, corresponding to an absorbance per unit path length of $2 \times 10^{-10}\,\text{cm}^{-1}$. Thus, the detection minimum improves five fold from pulsed to cw operation.

The largest contribution to the better detection limit of cw over pulsed operation observed in this study is the greater useful power of the cw laser. In pulsed operation, under optimal conditions, the average power at the detector is only $\sim 3\%$ of that available with cw operation. In the cw case, the laser output is 3 mW at a current of 530 mA and a base temperature of −9 °C (see Fig. 1). The cw power collected at the detector after passing through the multiple-pass cell is on the order of 0.05 mW, compared to 0.002 mW in pulsed mode.

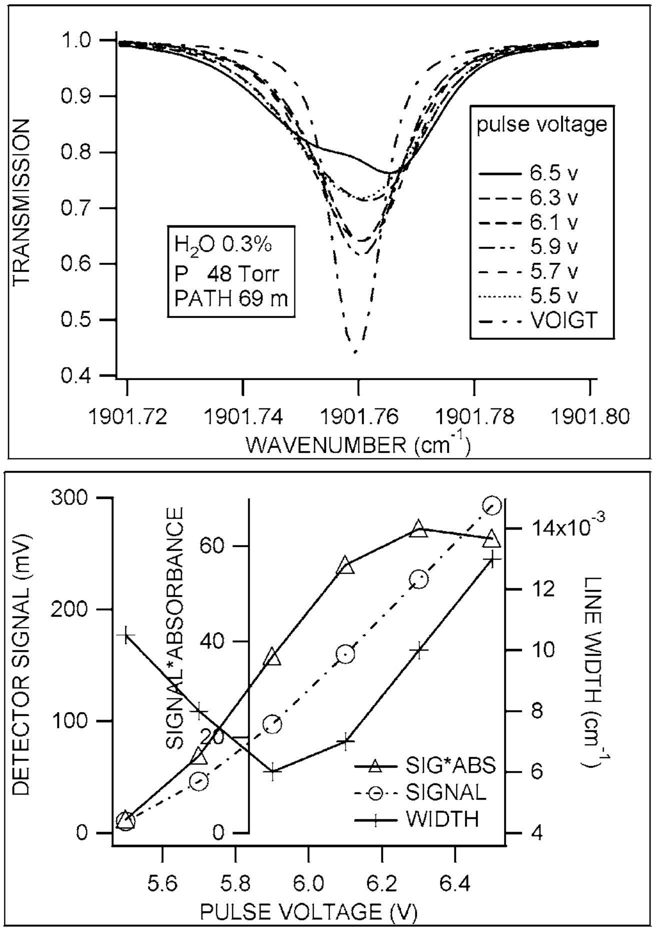

FIGURE 8 *Upper:* Effective absorption profile vs. voltage applied to the pulser, showing the effect of increasing laset line width. *Lower:* Laser line width, detector signal and signal × absorbance vs. pulser voltage

In pulsed mode, we operated the laser with the maximum pulse voltage commensurate with an acceptable level of spread of the laser line shape. While the laser power increases with applied voltage over threshold, the laser also ‘chirps’, or scans rapidly to spread and distort the absorption feature. Beyond some pulse voltage, there is a diminishing improvement in signal-to-noise for detecting the trace gas, since the peak absorbance decreases with increasing chirp width. In our spectral measurements the chirp is too rapid to directly observe. Rather, we observe broadened absorption lines that can be described with an effective laser line width. The dependence of effective laser line width, line shape, and power at the detector on pulse voltage is illustrated in Fig. 8. The data in the lower part of Fig. 8 is plotted with a horizontal axis of voltage applied to the pulser, a surrogate for the laser current, which is not directly measured. The line width has a minimum of 0.006 cm^{-1} (HWHM) at 0.5 V above threshold. The larger line width at low voltage is due to uncertainty broadening, since the pulse also becomes temporally narrower. The upper panel of Fig. 8 shows the distortion of a nearby single line (due to water vapor) as the laser pulse voltage, and laser line width, increases. At greater than 1 V above threshold, the laser line shape becomes asymmetrical and difficult to model in our fitting routines. An approximate figure of merit may be obtained from the product of the observed peak absorbance and the detector signal. As shown in the lower panel of Fig. 8, this parameter has a broad maximum at 0.8 V above threshold. We operate the laser in pulsed mode at ~ 1 V above threshold, giving a practical maximum to the useful intensity. The effective line width then is near 0.012 cm^{-1} (HWHM).

The line width in cw mode was determined previously to be $0.0004 \pm 0.0002\,\text{cm}^{-1}$ (HWHM) [7], by comparing experimental absorption spectra of the NO doublet at 1900.1 cm^{-1} to a simulation based on HITRAN [12] line positions and strengths. The observed cw laser line width is likely determined by electrical noise in the current controller or modulation circuit or by the temperature stability of the laser controller, and is therefore an upper limit to the instantaneous laser line width. Line widths of similar devices determined by heterodyne techniques without frequency tuning can be considerably narrower [14, 18, 19]. The laser line width in cw operation is a negligible contribution to the observed Voigt absorbance line profile in Fig. 8 at 40 Torr, so that there is larger peak absorbance for the same trace gas mixing ratio.

The difference in effective laser line width for pulsed vs. cw operation is illustrated by the NO doublet line shapes shown in Fig. 9. The spectra in Fig. 9 are obtained from ambient air sampled from the Aerodyne roof top, during two intervals with NO mixing ratios near 5 parts in 10^9. The peak absorbance for the NO doublet in cw mode at 46 Torr is 50% greater than in pulsed mode, although the area under the peak is the same in each case. The lower panel in Fig. 9 shows the reduction in noise with pulsed mode after averaging for 60 s. The cw mode spectrum shows less apparent reduction in the baseline structure, which is dominated by quasi-stable optical fringes rather than the random noise seen in the 1-s spectrum.

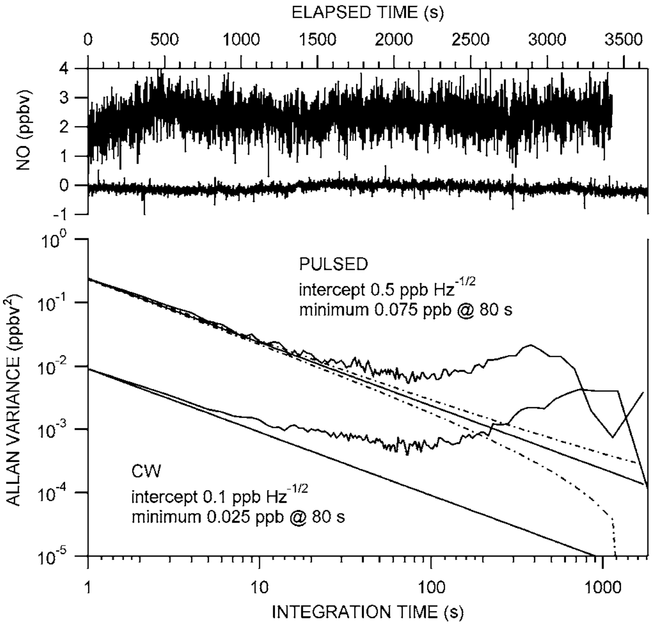

FIGURE 10 Allan plots with pulsed and cw modes of operation on NO line at 1900 cm^{-1} for 1-h time series on 'zero' air. *Upper part:* the upper time trace is for pulsed operation

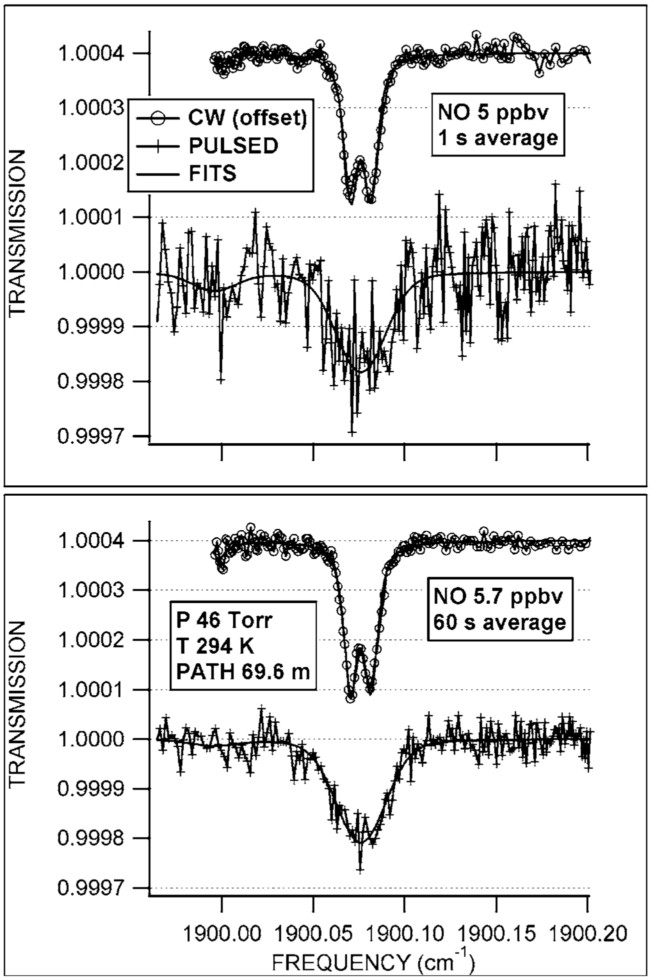

FIGURE 9 NO doublet comparing cw and pulsed modes of operation with 1-s spectra (*top*) and 60-s averaged spectra (*bottom*), contrasting random noise with pulsed mode and optical fringe structure with cw mode

The improvement in detection precision with averaging time in both cw mode and pulse mode is shown in the Allan variance plot [20, 21] in Fig. 10. The time series in the upper portion of the figure are obtained by flowing 'zero' air through the sample cell and accumulating spectra at 1 Hz for 1 h. The lower panel shows the decrease in variance with averaging time. The deviation noise at any time is given by the square root of the variance. Random noise from the detector and laser intensity will decrease with the square root of time until instrumental drifts at longer time scales begin to dominate. The left intercept in the Allan plot gives the short-term (1 Hz) noise. In pulsed mode the 1-Hz noise is 0.5 parts in 10^9 Hz$^{-1/2}$. In cw mode, the 1-Hz noise is 0.1 parts in 10^9 Hz$^{-1/2}$. The dominant contribution to the short-term (1 Hz) noise in pulsed mode is detector noise. In cw mode there are other optical noise sources (such as interference fringes) that dominate the short-term noise, with the detector noise only one-third of the total.

The minimum in the Allan plot shows the maximum useful averaging time. In pulsed mode the minimum variance corresponds to a standard deviation of 0.075 parts in 10^9 after 80 s of averaging time. In cw mode the minimum corresponds to 0.025 parts in 10^9 after 80 s. This minimum in the Allan plot with cw mode for NO corresponds to an absorbance of 1.3×10^{-6} or an absorbance per path length of 2×10^{-10} cm^{-1}.

A practical detection limit for NO with this system may be estimated from the Allan plot data. For a total averaging time of 100 s, including 50-s averaging of sample spectra and subtracting 50-s average background spectra, the 2σ detection limit in 100 s would be 0.07 parts in 10^9.

The limiting noise at the minimum in the Allan plot is controlled by different effects than those dominating the short-term noise. The noise limit in cw mode often is attributable to optical fringe instability, driven by thermal and mechanical drifts in the optical system. Laser source noise due to electrical instability in the current source and temperature instability of the laser base may also contribute to the noise limit. These effects are also applicable in pulsed operation, although high-frequency fringes from the multiple pass mirror system are less important with the pulsed system. Lower-frequency fringes occurring outside the multiple-pass cell will affect stability in both pulsed and cw modes. Good mechanical and thermal stability of the optical system are necessary to achieve the highest sensitivity and longer averaging times.

The cw detection limit in this study is ~ 3.5 times better than we previously reported, in a multi-pass cell of similar size [7]. The improved cw detection limit is due to several factors, including higher optical power at the detector and electronic filtering. The light level was higher than in earlier systems because of the more efficient collection of the off-axis ellipsoid. Adding a 100-kHz filter to the detector in the cw case creates a better match of the detection bandwidth to the signal time scales. The high-frequency structure in the signal is reduced by about one-half, and the concentration noise also falls by one-half.

In conclusion, a quantum cascade laser operating near room temperature with thermoelectric (TE) cooling has been used in both continuous-wave (cw) mode (-9 °C) and pulsed mode ($+45$ °C) to detect atmospheric nitric oxide using spectral lines at 1900.07 cm^{-1} (5.3 μm). The detection method uses direct absorption with rapid scan and sweep integration to derive quantitative concentrations in near real time. A low volume (0.5 l) reduced pressure (~ 40 Torr) multiple pass absorption cell allows sub-second time response. The pattern of reflections on the astigmatic cell mirrors has been designed to minimize optical interference fringes, which are substantially greater with cw than with pulsed operation. Detection precision for NO in air of 0.5 parts in 10^9 $\mathrm{Hz}^{-1/2}$ (1σ) is obtained in pulsed mode with an Allan variance minimum corresponding to 0.1 parts in 10^9 after 30-s averaging time. The precision in cw mode improves to 0.1 parts in 10^9 $\mathrm{Hz}^{-1/2}$ and 0.03 parts in 10^9 after 30-s averaging, corresponding to an absorbance per unit path length of 2×10^{-10} cm^{-1}. The better short-term detection limit in the cw case is largely due to the higher optical power at the detector. The useful power in the pulsed case is limited by chirp of the laser. At long time scales (30–100 s), the minimum detection limit available by averaging is limited by several drift and instability effects, which can be different in pulsed and cw operation. The five-fold advantage in detection limit of cw operation at 1 Hz is maintained at the longest useful averaging times. In pulsed operation, the effective laser line width produced by chirp was as great as 0.012 cm^{-1} (HWHM), enough to produce a broadened absorption profile when measured at 40 Torr. The cw laser line width of 0.0004 is significantly narrower than the absorption feature. The relative advantage of narrow line width cw operation is expected to be even greater for gases with complex and overlapping spectral features.

ACKNOWLEDGEMENTS The work at the University of Neuchâtel was supported in part by the National Center of Competence in Research (NCCR) ‘Quantum Photonics’. The work at Aerodyne Research was supported by the SBIR programs at the National Institute of Health (NIH) and the National Oceanic and Atmospheric Administration (NOAA). The authors would like to thank Sophie Brunner, Guillaume Vandeputte, Vanessa Piot, Lim-Vitou Nam, Sandra Hofmann (Alpes Lasers), and Nicolas Hoyler (University of Neuchâtel).

REFERENCES

1 M. Beck, D. Hofstetter, T. Aellen, J. Faist, U. Oesterle, M. Ilegems, E. Gini, H. Melchior, Science **295**, 301 (2002)

2 S. Blaser, D.A. Yarekha, L. Hvozdara, Y. Bonetti, A. Muller, M. Giovannini, J. Faist, Appl. Phys. Lett. **86**, 041 109 (2005)

3 J.S. Yu, S. Slivken, S.R. Darvish, A. Evans, B. Gokden, M. Razeghi, Appl. Phys. Lett. **87**, 041 104 (2005)

4 J.S. Yu, A. Evans, S. Slivken, S.R. Darvish, M. Razeghi, IEEE Photon. Technol. Lett. **17**, 1154 (2005)

5 Y.A. Bakhirkin, A.A. Kosterev, R.F. Curl, F.K. Tittel, D.A. Yarekha, L. Hvozdara, M. Giovannini, J. Faist, Appl. Phys. B **82**, 149 (2006)

6 B.W.M. Moeskops, S.M. Cristescu, F.J.M. Harren, Opt. Lett. **31**, 823 (2006)

7 D.D. Nelson Jr., J.B. McManus, S.C. Herndon, J.H. Shorter, M.S. Zahniser, S. Blaser, L. Hvozdara, A. Muller, M. Giovannini, J. Faist, Opt. Lett. **31**, 2012 (2006)

8 R. Jimenez, S. Herndon, J.H. Shorter, D.D. Nelson, J.B. McManus, M.S. Zahnsier, Proc. SPIE **5738**, 318 (2005)

9 G. Wysocki, A.A. Kosterev, F.K. Tittel, Appl. Phys. B **80**, 617 (2005)

10 G. Wysocki, M. McCurdy, S. So, D. Weidmann, C. Roller, R.F. Curl, F.K. Tittle, Appl. Opt. **43**, 6040 (2004)

11 S.C. Herndon, M.S. Zahniser, D.D. Nelson Jr., J.H. Shorter, J.B. McManus, R. Jimenez, C. Warneke, J.A. de Gouw, accepted for publication in J. Geophys. Res. (2006)

12 L.S. Rothman, D. Jacquemart, A. Barbe, D.C. Benner, M. Birk, L.R. Brown, M.R. Carleer, C. Chackerian Jr., K. Chance, L.H. Coudert, V. Dana, V.M. Devi, J.-M. Flaud, R.R. Gamache, A. Goldman, J.-M. Hartmann, K.W. Jucks, W.J. Lafferty, A.G. Maki, J.-Y. Mandin, S.T. Massie, J. Orphal, A. Perrin, C.P. Rinsland, M.A.H. Smith, J. Tennyson, R.N. Tolchenov, R.A. Toth, J. Vander Auwera, P. Varanasi, G. Wagner, J. Quantum Spectrosc. Radiat. Transf. **96**, 139 (2005)

13 J. Faist, D. Hofstetter, M. Beck, T. Aellen, M. Rochat, S. Blaser, IEEE J. Quantum Electron. **QE-38**, 533 (2002)

14 S. Blaser, L. Hvozdara, Y. Bonetti, A. Muller, A. Bächle, S. Jochum, S. Hansmann, T. Aellen, M. Giovannini, J. Faist, Proc. SPIE **6133**, 613 301 (2006)

15 D.D. Nelson, J.B. McManus, S. Urbanski, S. Herndon, M.S. Zahniser, Spectrochim. Acta **60**, 3325 (2004)

16 W.J. Riedel, Proc. IEEE **1433**, 179 (1991)

17 J.B. McManus, P.L. Kebabian, M.S. Zahniser, Appl. Opt. **34**, 3336 (1995)

18 M. Taubmann, T. Myers, B. Cannon, R. Williams, F. Capasso, C. Gmachl, D.L. Sivco, A.Y. Cho, Opt. Lett. **27**, 2164 (2002)

19 R. Maulini, D.A. Yarekha, J.-M. Bulliard, M. Giovannini, J. Faist, E. Gini, Opt. Lett. **30**, 2584 (2005)

20 D.W. Allan, Proc. IEEE **54**, 221 (1966)

21 P. Werle, R. Mucke, F. Slemr, Appl. Phys. B **57**, 131 (1993)